



Experimental evidence for statistical scaling and intermittency in sediment transport rates

Arvind Singh,¹ Kurt Fienberg,¹ Douglas J. Jerolmack,² Jeffrey Marr,¹ and Efi Foufoula-Georgiou¹

Received 7 December 2007; revised 9 August 2008; accepted 3 December 2008; published 3 March 2009.

[1] Understanding bed load transport fluctuations in rivers is crucial for development of a transport theory and for choosing a sampling interval for “mean” transport rates. Field-scale studies lack sufficient resolution to statistically characterize these fluctuations, while laboratory experiments are limited in scale and hence cannot be directly compared to field cases. Here we use a natural-scale laboratory channel to examine bed load transport fluctuations in a heterogeneous gravel substrate under normal flow conditions. The novelty of our approach is the application of a geometrical/statistical formalism (called the multifractal formalism), which allows characterization of the “roughness” of the series (depicting the average strength of local abrupt fluctuations in the signal) and the “intermittency” (depicting the temporal heterogeneity of fluctuations of different strength). We document a rougher and more intermittent behavior in bed load sediment transport series at low-discharge conditions, transitioning to a smoother and less intermittent behavior at high-discharge conditions. We derive an expression for the dependence of the probability distribution of bed load sediment transport rates on sampling interval. Our findings are consistent with field observations demonstrating that mean bed load sediment transport rate decreases with sampling time at low-transport conditions and increases with sampling time at high-transport conditions. Simultaneous measurement of bed elevation suggests that the statistics of sediment transport fluctuations are related to the statistics of bed topography.

Citation: Singh, A., K. Fienberg, D. J. Jerolmack, J. Marr, and E. Foufoula-Georgiou (2009), Experimental evidence for statistical scaling and intermittency in sediment transport rates, *J. Geophys. Res.*, 114, F01025, doi:10.1029/2007JF000963.

1. Introduction

[2] Measurements of bed load transport rates are fundamental to estimating material transport in a river, yet even defining a representative time period over which to sample is difficult due to the inherent variability and stochastic character of sediment transport. This variability is present over a wide range of scales, from the movement of individual grains [Iseya and Ikeda, 1987; Drake *et al.*, 1988; Nikora *et al.*, 2002; Schmeeckle and Nelson, 2003; Sumer *et al.*, 2003; Ancy *et al.*, 2008] up to the propagation of dunes and bars [Kuhnle and Southard, 1988; Gomez *et al.*, 1989; Cudden and Hoey, 2003; Jerolmack and Mohrig, 2005], even under steady flow conditions. Computed statistics of instantaneous bed load transport rates (flux) have shown that probability distributions are often skewed toward larger values [e.g., Gomez *et al.*, 1989], implying a high likelihood of extreme fluctuations, the prediction of which is essential

for protecting hydraulic structures and assessing the stability of riverine habitat [Yarnell *et al.*, 2006]. It has also been observed that the mean sediment flux depends on the time interval (sampling time) over which the mean is computed, and previous work has suggested that this time dependence is the result of large, infrequent transport events [see Bunte and Abt, 2005, and references therein].

[3] An analogous time dependence that has been more thoroughly studied is that of the sedimentary record, where apparent deposition rate (measured from two dated surfaces) diminishes rapidly with measurement duration in virtually all depositional environments [Sadler, 1981, 1999]. Models show that this scale dependence is a direct result of the statistics of transport fluctuations [e.g., Jerolmack and Sadler, 2007]. In the case of geologic rates the data have been assumed to obey simple scaling over a wide range of time scales; that is, the statistical moments can be fitted as power law functions of scale, with the exponents linear in moment order. This power law relationship provides a value for the Hurst exponent, H , which may be used to compare rates at one scale to rates at a different scale via a simple statistical transformation (see also section 5). However, many geophysical processes exhibit multiscaling (or multifractal behavior), which implies that a range of exponents (and not a single exponent) is required to describe the

¹St. Anthony Falls Laboratory and National Center for Earth-surface Dynamics, Department of Civil Engineering, University of Minnesota-Twin Cities, Minneapolis, Minnesota, USA.

²Department of Earth and Environmental Science, University of Pennsylvania, Philadelphia, Pennsylvania, USA.

changes in the probability density function (pdf) with scale. Examples include rainfall intensities [e.g., *Lovejoy and Schertzer, 1985; Venugopal et al., 2006b*], cloud structures [e.g., *Lovejoy et al., 1993; Arneodo et al., 1999a*], river flows [e.g., *Gupta and Waymire, 1996*], river network branching topologies [e.g., *Rinaldo et al., 1993; Marani et al., 1994; Lashermes and Fofoula-Georgiou, 2007*], braided river systems [e.g., *Fofoula-Georgiou and Sapozhnikov, 1998*], and valley morphology [e.g., *Gangodagamage et al., 2007*]. This rich multiscale statistical structure includes extreme but rare fluctuations (“bursts”) that occur inhomogeneously over time, giving rise to the so-called “intermittency” and leading to a nontrivial scaling of the statistical moments. A prime example of this is the velocity fluctuations in fully developed isotropic turbulence [e.g., *Parisi and Frisch, 1985; Frisch, 1995; Arneodo et al., 1999b*].

[4] To the best of our knowledge, bed load sediment transport series have not been analyzed before from the perspective of quantifying how the statistical moments of the series change with scale. In an early study, *Gomez et al. [1989]* acknowledged that the probability distribution of sediment transport rates depends on sampling time (scale) and extended the Einstein and Hamamori distributions to a scale-dependent form, without, however, attempting any scale renormalization. Knowledge of the variability inherent in bed load transport rates at all scales is essential for quantifying material flux, for designing appropriate measurement programs, and for comparison among different data sets and model predictions at different temporal and spatial scales. Also, quantifying the statistical structure of these fluctuations across scales may yield insight into the fundamental physics of sediment transport and provide a set of diagnostics against which to rigorously test competing theories and bed load transport models [see also *Ancey et al., 2006, 2008*].

[5] One would expect that the statistics of bed load sediment transport would relate in some way to the statistics of the fluctuations in bed elevation. Although river bed elevations have been analyzed much more than sediment fluxes and have been found to exhibit fluctuations across a wide range of scales, in both sandy [e.g., *Nikora et al., 1997; Nikora and Hicks, 1997; Jerolmack and Mohrig, 2005*] and gravelly [*Dinehart, 1992; Nikora and Walsh, 2004; Aberle and Nikora, 2006*] systems, the link between bed topography and sediment flux remains largely unexplored due to the difficulty in simultaneous data acquisition. Establishing a relationship between the statistics of bed elevations and sediment transport rates is important for effective modeling of river bed morphodynamics and also for understanding the physics of sediment transport. More practically, since bed elevation data are far easier to collect than sediment flux measurements, an understanding of how the statistics of the one variable relate to those of the other, at least over a range of temporal scales, could greatly facilitate estimating sediment transport rate in the field.

[6] To address these issues we present here an analysis of data from a unique experimental laboratory setup capable of mimicking transport conditions in the field (see section 3). High-resolution, long-duration time series of sediment transport rates and bed elevation were simultaneously collected in a suite of experiments with a heterogeneous gravel bed. We use the multifractal formalism, originally

developed for fluid turbulence [*Parisi and Frisch, 1985; Frisch, 1995; Muzy et al., 1994*], to quantify the “roughness” (the average strength of local burstiness in the signal) and the “intermittency” (the temporal variability or heterogeneity of bursts of different strengths) and relate those geometrical quantities to the statistics of sediment flux and bed topography over a range of time scales. (Note that throughout the paper the term “roughness,” as defined mathematically via the strength of local singularities, refers to the signal roughness being that sediment transport rates or bed elevation fluctuations and it is not to be confused with other uses of the term roughness such as bed roughness or hydraulic roughness.) We substantiate the findings of *Bunte and Abt [2005]* that mean sediment transport rate diminishes with increasing sampling time at low bed stress (slightly above critical) but does the opposite for high-transport conditions, and we relate this reversal in trend to the influence of large-scale bed forms. Our analysis also allows characterization of the sampling time dependence of all of the statistical moments, allowing thus the prediction of extremes at small scales from the statistics at larger scales.

2. Description of Experiments

2.1. Experimental Setup

[7] The experiments reported here were conducted in the Main Channel facility at the St. Anthony Falls Laboratory, University of Minnesota, as part of the StreamLab06 project undertaken by the National Center of Earth-surface Dynamics (NCED) [*Wilcock et al., 2008*]. StreamLab06 was an 11 month multidisciplinary laboratory channel study focused on various aspects of ecogeomorphology in gravel bed streams. Five separate projects were conducted as part of StreamLab06 and an extensive data set was collected including hydraulic conditions (discharge, water slope, bed slope, depth average velocity, and flow field), morphological conditions (bed topography, bar locations and shapes, photo images of the bed), sediment transport characterization (continuous sediment flux, recirculation grain size information), water chemistry (temperature, dissolved oxygen, nutrient concentrations) and biological conditions (heterotrophic respiration, biomass accumulation, nutrient processing rates). For the work presented here, we focus on bed topography and sediment flux data collected in the first of the five StreamLab06 projects, which focused on ground truth testing of various conventional and surrogate bed load monitoring technologies.

[8] The Main Channel is 2.74 m wide and has a maximum depth of 1.8 m. It is a partial-recirculating channel with the ability to recirculate gravel while the water flows through the channel without recirculation. Water for the channel was drawn directly from the Mississippi River, with a maximum discharge capacity of 8000 L/s. Water discharge was controlled by a sluice gate situated at the head end of the facility while flow depth was regulated by a sharp-crested weir located at the downstream end of the channel. The channel has a 55-m-long test section and in the experiments reported here a poorly sorted gravel bed extended over the last 20 m of this test section. Short, 0.4-m-high bulkhead walls were located upstream and downstream of the test section and served to contain the gravel bed material. The gravel used in these experiments had a broad



Figure 1. Weighing pans located at the downstream end of the experimental Main Channel.

particle size distribution characterized by $d_{50} = 11.3$ mm, $d_{16} = 4.3$ mm and $d_{84} = 23.1$ mm [see also *Fienberg et al.*, 2008]. The thickness of the gravel bed at the start of run was approximately 0.45 m.

[9] The Main Channel was equipped with a sediment flux monitoring system that provided the ability to collect high-resolution, long-duration data sets of sediment transport dynamics using field-scale gravel particle sizes and transport rates. The sediment flux and recirculation systems were colocated in the channel at the downstream end of the 20-m test section. The flux monitoring system was composed of five adjacent, identical aluminum weighing pans (positioned 0.54 m apart) that spanned the width of the channel and independently measured the submerged weight of the gravel intercepted by the bed load trap (see Figure 1). Each pan could accommodate up to 76-mm-diameter particles and hung from an aluminum frame that extended from its sides to a load cell connected to the ceiling above the Main Channel (see Figure 2). The system used load cells manufactured by Interface Advanced Force Measurement (SM-250) that had a capacity of 113 kg and were accurate to ± 45 gram force. As a safety margin to avoid exceeding the capacity of the weighing pan system, the pan rotation that voided each bin's contents was triggered at a user-specified net weight, which in our case was set to 20 kg force (kg f).

[10] Removable stainless steel cover plates with 45-cm by 15-cm slots served to funnel the intercepted bed load downward into the pans. The pans (also referred as drums) were constructed of aluminum and had three radial baffles welded to a common 3.8-cm diameter hub and to two 81.3-cm-diameter end plates. They were oriented horizontally and transverse to the channel under the sediment trap. The three radial baffles formed two adjacent 120° "V"-shaped bins, each of which had a capacity of 62 L. The submerged weight of sediment in a bin at maximum capacity was 62 kg f. Each pan operated independently using a tipping bucket arrangement with "tips" consisting of alternating clockwise and counterclockwise 120° rotations. When the sediment mass in a pan reached a specified threshold, an air cylinder either extended or retracted, causing the pan to rotate 120 degrees. This action resulted in dumping the contents of one bin and repositioning the adjacent empty bin under the funnel to continue collecting bed load. In this manner, all bed load was continuously captured and weighed in the five independently operating pans.

[11] Bed load material that was transported out of the test section fell by gravity into the pans and incrementally added

to the weight of the pan which was recorded every 1.1 s. Material dumped out of the pans was collected in a large hopper located underneath the pans, which also served as the material source for the recirculation system. The rate of gravel removal out of this hopper, and delivery to the upstream end of the channel via a large pump, was manually set by adjusting the rotation speed of a large helix, which served to push gravel laterally out of the hopper and into the recirculation line. In this way, the collection hopper and helix served to buffer small fluctuations in sediment flux out of the test section, providing a more steady "feed-type" delivery of sediment to the upstream end. Because the physical size of the collection hopper was finite, the auger speed (and hence upstream input sediment feed rate to the test section) was manually adjusted periodically to maintain storage in the hopper. In other words, an auger rate set too high could potentially remove material faster than the test section would deliver resulting in emptying of the hopper. Conversely, an auger rate set too low would result in overfilling of the hopper. We used periodic visual observations of the fill level in the collection hopper to inform our manual adjustments of the auger speed. Slight adjustments to auger speed were necessary every 30–60 min and very rarely did the system collection hopper empty or overflow meaning that the feed rate out of the collection hopper was in balance with the long-term flux of bed load out of the test section.

[12] The experimental setup also included five stationary 2.5-cm-diameter, submersible sonar transducers deployed 0.95 m below the water surface and 0.95 m upstream of each pan. The sonar transducers, mounted to the end of rigid 1.5-cm steel tubes and directed perpendicular to the bed, were used to collect continuous temporal bed elevation information upstream of the each pan. Sonar data was sampled at every 10 sec with a vertical precision of ~ 1 mm. The acquisition times for the bed elevation and sediment accumulation data were based on precisely synchronized clocks allowing the two data sets to be analyzed together. Water temperature was also measured using YSI thermistor capable of measuring up to $\pm 0.1^\circ\text{C}$. Water temperature for the two runs studied in this research averaged 3.0°C .

[13] Measurements of bed elevation and sediment transport were taken over a range of discharges corresponding to

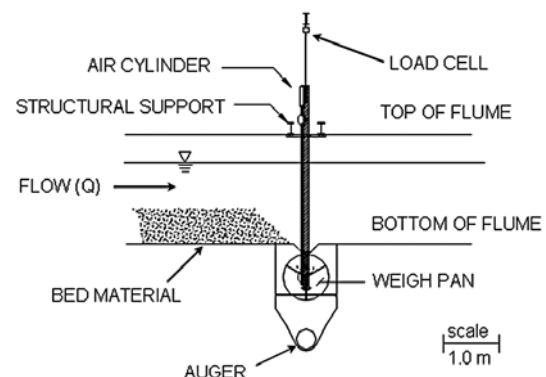


Figure 2. Side view schematic of a pan and sediment recirculation system in the Main Channel.

Table 1. Hydraulic Conditions for the Two Studied Discharges^a

Q _w (L/s)	Depth (m)	V (m/s)	h _R (m)	S _w (%)	τ^*_{b}	T _{mean} (°C)
4300	1.3	1.20	0.67	0.23	0.085	3.5
5500	1.3	1.54	0.67	0.53	0.196	2.7

^aQ_w is design water discharge for the run; depth is average depth of flow in test section; v is velocity of flow; h_R is hydraulic radius; S_w is water surface slope; τ^*_{b} is dimensionless Shields stress (computed using hydraulic radius); and T_{mean} is mean water temperature.

different bed shear stresses. Bed shear stress is often characterized in terms of the dimensionless Shields stress, τ^*_{b} . For steady, uniform flow it may be approximated as $\tau^*_{b} = h_R S / R d_{50}$, where h_R and S are the hydraulic radius and channel slope, respectively, and $R = 1.65$ is the relative submerged density of silica. In the analysis presented here, we report on two different discharges: a low-discharge case, with a discharge of 4300 L/s, corresponding to a dimensionless bed stress of about twice the critical value (Shields stress, $\tau^*_{b} = 0.085$ using median diameter) and a high discharge, 5500 L/s, corresponding to a bed stress about five times the critical value (Shields stress, $\tau^*_{b} = 0.196$); see Table 1 for relevant hydraulic parameters. (Note that the critical Shields stress (also known as Shields number) was estimated to be 0.047 [Meyer-Peter and Müller, 1948].)

[14] For both bed stress conditions, the channel was allowed to run prior to data collection such that a dynamic equilibrium was achieved in transport and slope adjustment of the water surface and bed. Determination of the dynamic

equilibrium state was evaluated by checking the stability of the 60 min average total sediment flux at the downstream end of the test section. Using the pan accumulation data, the acquisition software computed a 60 min mean of sediment flux in all five pans. Dynamic equilibrium was reached when variation in this value became negligible. In other words, when the average of the previous 60 min of instantaneous flux values computed from the pan data stabilized, we determined the channel to be in dynamic equilibrium and proceeded with formal data collection and sampling.

[15] The bed load sediment accumulation series and the corresponding bed elevation series were then recorded over a span of approximately 20 h for each experiment. Figures 3a and 3b display the time series of sediment accumulation over 2 min and 10 min intervals, respectively, for pan 4, and Figure 3c the corresponding bed elevation series (recorded by the sonar transducer immediately upstream of pan 4) for the low-discharge conditions over a period of 10 h. Figure 4 shows the same series for the high-discharge conditions. Considering the bed elevation series, it can be observed that the low bed stress run (Figure 3c) produced a channel bed with only limited topographic variation, i.e., without obvious large-scale structures in the bed (the standard deviation in the bed is 10.1 mm, compared to a d_{50} grain size of 11.3 mm). However, the higher stress run (Figure 4c) generated substantial bed variability at large scale in the form of dunes, with intermediate to particle-scale fluctuations superimposed on these larger-scale features. In this study we focus on

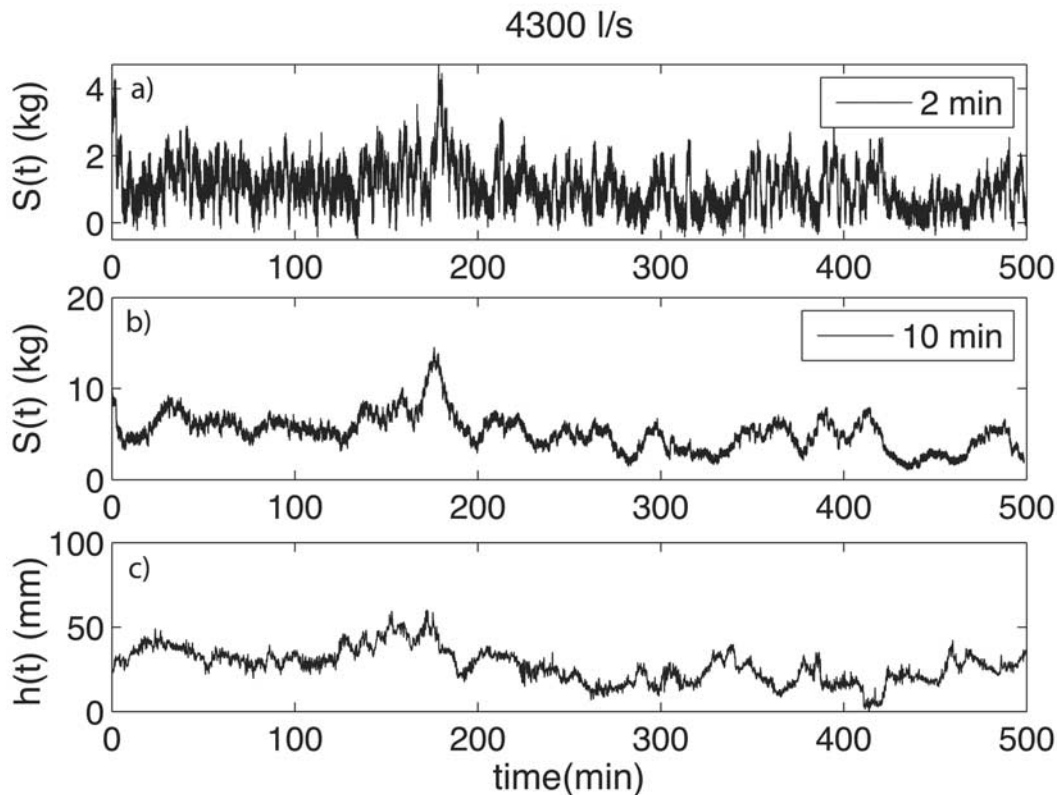


Figure 3. Low-transport conditions (flow rate 4300 L/s). Bed load sediment transport series accumulated every (a) 2 min and (b) 10 min and (c) the corresponding series of gravel bed elevations.

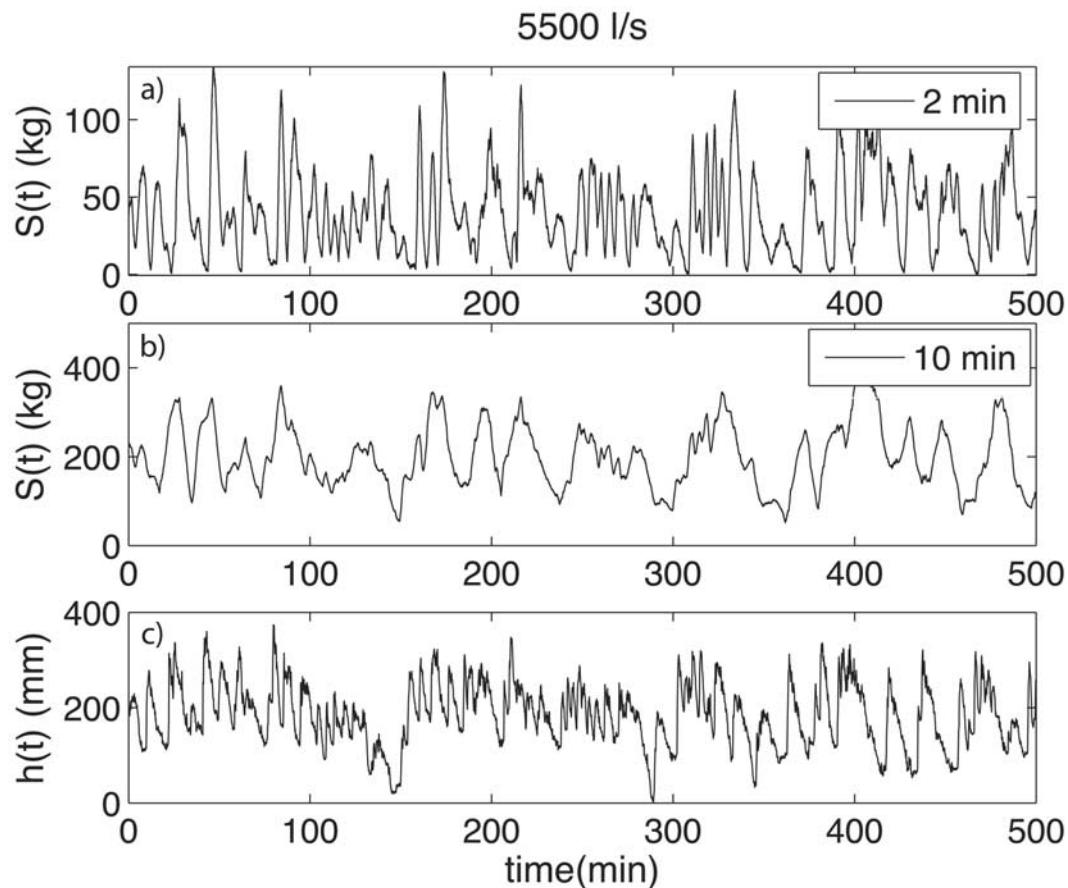


Figure 4. High-transport conditions (flow rate 5500 L/s). Bed load sediment transport series accumulated every (a) 2 min and (b) 10 min and (c) the corresponding series of gravel bed elevations.

comparing these two runs using the multiscale analysis techniques described in section 3.

2.2. Sources of Error in the Data

[16] One source of error in the accumulated sediment series was the tipping events of the pans. To account for this, the raw sediment accumulation data were preprocessed prior to the analysis presented here. The preprocessing involved removal of pan dumping events from the data and translating the data set into a continuous accumulation of sediment time series for each pan over the duration of the experiment. A single tipping event required the removal of no more than eight data points (~ 8.8 s) from the record. To get the final time series of accumulated sediment transport, the time series prior to the tipping event was left unchanged, the tipping event was removed from the series, and all subsequent points were shifted backward in time to create a continuous time series as though the tipping event never occurred. Overall, the data affected by the pan tipping constituted less than 0.15% of the total data record and is, thus, negligible.

[17] There were other sources of error, however. Sediment accumulation data in the pans should increase monotonically, when corrected for tipping of the scales as discussed above. At the resolution of our measurements (approximately 1 s), however, sediment accumulation showed negative excursions which would imply negative bed load flux, which is not physically possible given the

experimental setup [see *Fienberg et al.*, 2008, Figure 3]. These errors have been attributed to (1) the fluctuating water surface over the pan, (2) the natural oscillation of the pans after being hit by the falling gravel, and (3) to the vibration caused by the large gravel recirculation pump which was placed near to the pans. This error makes the raw sediment data at small time scales (from 1 s up to approximately 1–2 min accumulations) unusable. As a check, we computed distributions of sediment flux values averaged over different time scales and found that data averaged over less than 2 min showed negative values, supporting the contention that scales smaller than 2 min are error prone. Also, although there were five pans, pans 1 and 5 (Figure 1) were not used in order to avoid data potentially impacted by wall effects.

[18] Bed elevation data were substantially less error prone, due to the acoustic (rather than mechanical) nature of the measurements. Our multiscale analysis showed a small noise regime which was only a small factor larger than the sampling interval of 10 s.

3. Roughness, Intermittency, and Statistical Scaling

3.1. Characterizing Signal Roughness and Intermittency

[19] Previous authors [e.g., *Gomez et al.*, 1989; *Ancey et al.*, 2006] have observed and documented high fluctuations in bed load sediment transport rates or particle counts at

short time scales and have described these series as “intermittent.” In these and other studies it has also been noted that as flow rate increased, the sediment transport was seen to be “smoother” or more continuous, whereas at low flow rates it was “rougher” or more “bursty.” These terms have been used in a qualitative way to describe the presence (or absence) of sudden bursts of sediment or high fluctuations at short time scales that arise from the stochastic nature of the transport and the collective behavior of particle dynamics.

[20] In this paper the “roughness” and “intermittency” of the sediment transport series are mathematically defined, allowing a more precise quantification of the nature of the fluctuations in bed load sediment at small time scales. A mathematical characterization of the strength of local fluctuations in a function $X(t)$ is given by the Hölder or singularity exponent $h(t_0)$, defined at any point t_0 to be the largest exponent such that:

$$|X(t) - X(t_0)| \leq C|t - t_0|^{h(t_0)}, \text{ as } t \rightarrow t_0 \quad (1)$$

where C is a constant. This definition holds for $0 \leq h \leq 1$, but it can be generalized to $h > 1$, as discussed in section 3.3 [see also *Muzy et al.*, 1994]. The Hölder exponent gives a local measure of the smoothness or degree of differentiability of the function $X(t)$: a value of $h(t_0) \geq 1$ indicates that the function is smooth at t_0 , in the sense that it is at least once differentiable at the point t_0 , whereas a function with $h(t_0) = 0$ is so rough that it is discontinuous at that point. Between these extremes, a value of $0 < h(t_0) < 1$ means that the function is continuous but not differentiable at t_0 , with a higher h value (closer to 1) implying that the function is “smoother” or more regular, and a lower h value (closer to zero) implying that the function is “rougher” or more irregular.

[21] Having established a measure of local (point-wise) roughness in a signal, it is natural to ask what kind of $h(t_0)$ values are present in an observed time series, and how they are distributed. If we denote the set of all points in the function $X(t)$ with a particular value of Hölder exponent h as:

$$\Omega(h) = \{t_0 : h(t_0) = h\} \quad (2)$$

then, in general, for a multifractal function these sets of points are interwoven fractal sets whose distribution can be characterized by the so-called singularity spectrum $D(h)$, defined as

$$D(h) = \text{Dim}_H(\Omega(h)) \quad (3)$$

where Dim_H is the Hausdorff dimension of the fractal set [e.g., *Schroeder*, 1991]. In other words, the singularity spectrum $D(h)$ describes the relative frequency of occurrence of local abrupt fluctuations (singularities) with strength h . In a one-dimensional function like a time series, the value of h corresponding to the peak of the singularity spectrum indicates the most frequently occurring singularity or fluctuation strength. (Note that if $D(h)$ is symmetric, which is a good approximation for most signals, then this value characterizes the “average roughness” of the signal as it coincides with the arithmetic mean of the local singularities h .) The range of h over which $D(h) \geq 0$, or

the spread of the singularity spectrum, reflects the temporal heterogeneity of the local singularities; that is, it measures the degree of clustering in the abrupt local fluctuations of various strengths. Simply put, a signal with a wide $D(h)$ will have sparse regions where the strength of the local fluctuations is much greater than (or much less than) the mean fluctuation strength, and hence will display infrequent but exceptionally large “bursts” at small scales embedded within bursts of lesser strength; that is, the signal will be very “intermittent.” On the other hand, a $D(h)$ spectrum which is just a spike, i.e., $D(h) = 1$ at $h = H$ and zero elsewhere, indicates a signal which exhibits one strength of singularity only, H also called the Hurst exponent, which is homogeneously distributed throughout the signal (in this case the signal has zero intermittency). It is noted that H , which is a local measure of variability, provides different information than the standard deviation of a signal, which is a global measure of variability; in other words two signals with the same standard deviation can have considerably different values of H [e.g., see *Turcotte*, 1997].

3.2. Multiscale Analysis

[22] While the spectrum of singularities $D(h)$ can be used to describe the “roughness” and “intermittency” of a signal, it can be difficult to estimate it directly from the data. An interesting mathematical result (the so-called multifractal formalism [*Parisi and Frisch*, 1985; *Muzy et al.*, 1994]) establishes that $D(h)$ relates to how the probability density function (pdf), or equivalently the statistical moments, of the signal fluctuations changes with scale. Let the fluctuation $S(t_0, a)$, at any time t_0 and scale a , be defined as

$$S(t_0, a) = X(t_0 + a) - X(t_0) \quad (4)$$

and the statistical moments of the absolute values of these fluctuations by

$$M(q, a) = \langle |S(t_0, a)|^q \rangle \quad (5)$$

where angle brackets denote expectation over time. For a process that exhibits statistical scale invariance, the statistical moments of the fluctuations behave as a power law function of scale:

$$M(q, a) \sim a^{\tau(q)} \quad (6)$$

where $\tau(q)$ is the so-called spectrum of scaling exponents and is a function of the moment order q . Thus if the series exhibits scale invariance, the function $\tau(q)$ completely describes the manner in which the statistical moments of the pdf of fluctuations varies with scale.

[23] It is the scaling function $\tau(q)$ that can be used to retrieve the spectrum of singularities $D(h)$. The precise transform between these two representations is given by the Legendre transform [*Parisi and Frisch*, 1985; *Muzy et al.*, 1994]:

$$D(h) = \min_q [qh - \tau(q) + 1] \quad (7)$$

In this way the spectrum of singularities describing the average roughness and intermittency of the signal can be

estimated through the scaling properties of the statistical moments of the signal fluctuations.

3.3. Generalized Fluctuations and the Wavelet Transform

[24] Although the fluctuations $S(t_0, a)$ of a time series can be computed by directly taking the first-order increments, as in equation (4), calculating the statistical moments in this way (which gives rise to the so-called structure function approach) has some limitations. First, these fluctuations can be corrupted by small-scale noise (since observations are used directly without local smoothing); in addition, they do not remove higher-order nonstationarities (it is easy to show that the first-order increments remove only constant level trends); and finally, they cannot estimate singularity strengths $h > 1$. To overcome these limitations, the continuous wavelet transform can be used to define generalized fluctuations in the time series [e.g., see *Arneodo et al.*, 1995; *Jaffard*, 1997; *Venugopal et al.*, 2006a; *Lashermes and Foufoula-Georgiou*, 2007]. In this framework we redefine the (generalized) fluctuations $S(t_0, a)$ to be

$$S(t_0, a) = \int_{-\infty}^{\infty} \psi_{a,t_0}(t) X(t) dt \quad (8)$$

where $\psi_{a,t_0}(t)$ is a “differencing function,” as for example, the first derivative of a Gaussian function. In particular ψ_{a,t_0} is a wavelet resulting from shifting and scaling a mother wavelet $\psi(t)$, such that,

$$\psi_{a,t_0}(t) = \frac{1}{a} \psi\left(\frac{t-t_0}{a}\right) \quad (9)$$

where t_0 is the location and a is the scale parameter. For the continuous wavelet transform to be invertible, the mother wavelet must satisfy the invertibility condition $\int_{-\infty}^{\infty} t\psi(t)dt = 0$ i.e., it must have a zero mean (which makes it a kind of local differencing function; e.g., see *Mallat* [1998] or *Kumar and Foufoula-Georgiou* [1997]). A commonly used mother wavelet is the family of Gaussian wavelets defined as the N th-order derivatives of a Gaussian function $g_0(t)$, i.e., $g_N(t) = (d^N/dt^N) g_0(t)$, modulus a proper multiplicative factor to ensure correct normalization. Defining the fluctuations $S(t_0, a)$ using the first-order derivative of the Gaussian function can be seen as computing first-order increments of the series after the series has been locally smoothed with a Gaussian kernel or, equivalently, as computing first-order increments and then performing a smoothing (weighted averaging). (This can be easily deduced from the convolution theorem [see also *Lashermes et al.*, 2007].) Similarly, defining multiresolution coefficients using $g_N(t)$ can be considered as smoothing the series with a moving Gaussian window, followed by N th-order differencing (the standard deviation of the Gaussian function determines the “scale” at which the smoothing and thus differencing is done [see *Lashermes and Foufoula-Georgiou*, 2007]). The smoothing operation removes the noise and the higher-order differencing removes nonstationarities from the signal, rendering the wavelet-based

generalized fluctuations appropriate for characterization of statistical scaling [e.g., see *Muzy et al.*, 1994].

[25] One property that should be considered when choosing an appropriate mother wavelet for defining the multiresolution coefficients is the number of vanishing moments. Note that the mother wavelet is said to have N vanishing moments if

$$\int_{-\infty}^{\infty} t^k \psi_o(t) dt = 0$$

for $0 \leq k < N$. The Gaussian wavelet $g_N(t)$, defined above as the N th derivative of the Gaussian, can be easily shown to have N vanishing moments. Defining multiresolution coefficients with a mother wavelet which has N vanishing moments can be shown to remove from the series an additive polynomial trend of degree less than N [e.g., see *Kumar and Foufoula-Georgiou*, 1997]. Therefore, the wavelet-based multiscale analysis proposed here renders the fluctuation series stationary if one chooses a wavelet with more vanishing moments than the degree of nonstationarity in the data. In practice, the degree of nonstationarity of the data series is not known in advance, so one applies the wavelet transform $g_N(t)$ with increasing values of N until the results of the analysis do not vary with N : this will imply that the order has been chosen large enough to remove any nonstationarities. The correct selection of multiresolution coefficients is important for a meaningful multifractal analysis as has been recently demonstrated by *Lashermes and Foufoula-Georgiou* [2007]. For example, using standard fluctuations (first-order differences) to analyze a nonstationary signal will result in a spurious estimate of $H = 1$ misleading one to assume that the signal is smooth and differentiable.

[26] In this study, the fluctuations, $S(t_0, a)$, of the bed load sediment and bed elevation series at various scales were computed using the wavelet transform (equation (8)) with the wavelet $g_3(t)$, since this was the lowest-order wavelet able to remove all nonstationarities from the sediment transport series (a lower-order wavelet g_2 proved sufficient for the bed elevation series but the use of the higher-order wavelet g_3 does not alter the results; this is discussed in more detail in section 4). The moments $M(q, a)$ were then estimated using equation (5), and the scaling exponents $\tau(q)$ computed from the log-log linear relationships (equation (6)) over the scaling range. This in turn allowed the calculation of the singularity spectrum $D(h)$ via equation (7).

3.4. Scale Dependence of the pdf of the Fluctuations

[27] The scaling exponents $\tau(q)$ are not only of interest for calculating the singularity spectrum $D(h)$, but also for describing how the pdf of the fluctuations depends on scale. As discussed in section 3.2, the statistical moments $M(q, a)$ in equation (5) describe how the fluctuations of a process change with scale and, for a scale-invariant process, this change is captured in the $\tau(q)$ curve. In the case of simple scaling, the scaling exponent function is linear in moment order, i.e., $\tau(q) = qH$ for some constant H (called the Hurst exponent), which can be shown to imply that the pdf of the fluctuations at scale a , $P_a(S) \equiv P(S(t, a))$, is related to the

pdf at another scale a by [e.g., see *Arneodo et al.*, 1997; *Venugopal et al.*, 2006a]

$$P_{a'}(S) = \left(\frac{a}{a'}\right)^{-H} P_a\left(\left(\frac{a}{a'}\right)^{-H} S\right) \quad (10)$$

Note that the normalizing factor $(a/a')^{-H}$ is a deterministic kernel that depends on H and the ratio of scales (not each scale individually). As this type of statistical scaling behavior is controlled by a single parameter only, it is referred to as monoscaling. Note that equation (7) implies that in the monoscaling case $D(h) = \delta(h - H)$, i.e., the only Hölder exponent with dimension greater than zero is $h = H$, and the function is completely uniform in its roughness, i.e., not intermittent, at small scales.

[28] In the more general case of multiscaling, the scale invariance relation (equation (6)) still holds, but $\tau(q)$ is not linear but a concave function of the moment order q . In this case, the pdf of the fluctuations does not maintain its shape between two different scales but changes continuously via convolution with a kernel that depends on the ratio of scales [*Arneodo et al.*, 1999b; *Venugopal et al.*, 2006a]. The generalization of equation (10) for multifractals is obtained [*Castaing et al.*, 1990] by considering that H is not a constant but has a probability density function $\rho(h)$. In this case, expression (10) becomes

$$P_{a'}(S) = \int_{-\infty}^{\infty} \rho(h) \left(\frac{a}{a'}\right)^{-h} P_a\left(\left(\frac{a}{a'}\right)^{-h} S\right) dh \quad \text{for } a' < a \quad (11)$$

In general, the pdf of the fluctuations is expected to widen and have fatter tails as the scale decreases. In turbulence, for example, the above transformation renormalizes the almost Gaussian pdf of turbulent velocity fluctuations at very large scales to a thick-tailed pdf at small scales. It is noted that the probability density involved in the renormalization of the pdf's is related to the spectrum of singularities $D(h)$, $\rho(h) \propto a^{-D(h)}$, and reflects the presence of Hölder exponents of various strengths which are inhomogeneously distributed throughout the signal (see *Frisch* [1995] and also *Venugopal et al.* [2006a] for a discussion of the equivalency of the geometrical and statistical interpretations). The pdf rescaling of (11) can be expressed in a convolution form as

$$P_{a'}(S) = \int_{-\infty}^{\infty} G_{aa'}(u) e^{-u} P_a(e^{-u} S) du \quad \text{for } a' < a \quad (12)$$

where $u = h \ln(a/a')$ and $G_{aa'}(u) = \rho[u \ln(a/a') / \ln(a/a')]$. This implies that the pdf at scale a' can be expressed as a weighted sum of dilated pdf's at larger scales $a > a'$. The kernel $G_{aa'}(u)$ is called the propagator and can be estimated from the data (see *Castaing et al.* [1990] for the theory and *Venugopal et al.* [2006a] for an application to high-resolution temporal rainfall series). Once the propagator is known, a known pdf at any scale can be used to derive the pdf at any smaller scale via equation (12).

[29] To gain better insight into how the $\tau(q)$ (or $D(h)$) curve controls the pdf change over scales, let us consider the coefficient of variation, C_v , which is the ratio of the standard

deviation to the mean, $C_v = \sigma/\mu$. For a monoscaling process, this ratio would be constant with scale, as both the mean and standard deviation are rescaled equally, as shown by equation (6). In a multiscaling situation, however, the increasing width of the pdf leads to C_v increasing with decreasing scale. The precise behavior of C_v with scale can be seen by noting that $C_v^2 + 1 = M(2, a)/M(1, a)^2$, so that for a multiscaling process, equation (6) implies $(C_v^2 + 1) \sim a^{\tau(2) - 2\tau(1)}$. In other words, $\tau(2) - 2\tau(1)$ characterizes the (second order) relative stretching of pdf's across scales, and its magnitude is also a measure of deviation from monoscaling. Similar relationships can be worked out for higher-moment ratios. As we will see for the sediment transport series, C_v significantly depends on scale, attesting to the presence of multiscaling.

3.5. Parameterizing the Scaling Properties and Singularity Spectrum

[30] While knowing the $\tau(q)$ (or $D(h)$) curve completely characterizes the scale dependence of the pdf's of fluctuations, for practical purposes it is often desirable to parameterize these curves concisely. Assuming an analytic form of the $\tau(q)$ curve, the simplest parameterization for multiscaling is to extend the linear model of $\tau(q)$ used for monoscaling to a quadratic model, that is,

$$\tau(q) = c_0 + c_1 q - \frac{c_2}{2} q^2 \quad (13)$$

In this parameterization, the constant $c_0 = \tau(0)$ is the scaling exponent of the zeroth-order moment, which will be equal to zero if the support of the field under analysis fills the space, as we see for both sediment flux and bed elevation. This leaves two parameters to describe the (multi)scaling: the parameters c_1 and c_2 control the scaling of all the moments and the change in shape of the pdf with changing scale. The two parameters c_1 and c_2 in (13) can be estimated by fitting a quadratic function to the empirical $\tau(q)$ curve, or via a more robust methodology called the cumulant analysis (see *Delour et al.* [2001] and *Venugopal et al.* [2006a] for an application to rainfall series).

[31] For such a quadratic $\tau(q)$, it can be shown from equation (7) [e.g., *Venugopal et al.*, 2006a] that the spectrum of singularities is also quadratic, with

$$D(h) = 1 - \frac{1}{2c_2} (h - c_1)^2 \quad (14)$$

This shows that the most frequently occurring value of the Hölder exponent (peak of the $D(h)$ curve), and hence the mean roughness/smoothness of the function, is given by the parameter c_1 (note that $D(h) = 1$ and $D(h)$ in (14) is symmetric around c_1). Alternatively, c_2 provides a measure of the spread of the $D(h)$ curve and hence prescribes the degree of intermittency. For this reason, c_2 is referred to as the "intermittency coefficient." The limiting case of $c_2 = 0$, that is the case of a monofractal, leads to a delta function $D(h) = \delta(h - c_1)$, and hence gives a single Hölder exponent $H = c_1$ (the same exponent H as in equation (10)). This means there is no intermittency: the function will have the same degree of local roughness (irregularity) everywhere. For a multifractal ($c_2 > 0$), however, a range of local

Table 2. Multifractal Parameters Estimated for Low and High Flows Using Different Gaussian Wavelets^a

Shields Stress	Pan	Scaling Range (min)	Wavelet	c_1	c_2
$Q = 4300 \text{ L/s}$					
0.085	2	1.2–10	g2	0.57	0.12
	2	1.2–10	g3	0.56	0.14
	2	1.2–10	g4	0.54	0.12
	3	1.2–10	g2	0.52	0.11
	3	1.2–10	g3	0.49	0.13
	3	1.2–10	g4	0.48	0.13
	4	1–8	g2	0.49	0.10
	4	1–8	g3	0.47	0.10
$Q = 5500 \text{ L/s}$					
0.196	2	1–10	g2	1.04	0.09
	2	1–10	g3	1.07	0.09
	2	1–10	g4	1.09	0.10
	3	1–10	g2	1.04	0.11
	3	1–10	g3	1.07	0.10
	3	1–10	g4	1.09	0.11
	4	1–10	g2	1.09	0.11
	4	1–10	g3	1.12	0.11
4	1–10	g4	1.14	0.11	

^aSee text for definitions.

fluctuation strengths will be inhomogeneously distributed throughout the signal, with the minimum and maximum Hölder exponents given by $h_{\min/\max} = c_1 \mp \sqrt{2c_2}$ (where the $D(h)$ curve crosses below 0). So with increasing c_2 there is a wider range of local fluctuation strengths present in the signal, and hence a greater degree of intermittency.

4. Results

4.1. Sediment Transport Scaling

[32] Bed load sediment transport fluctuations were analyzed using the multifractal formalism. Fluctuations were computed by applying a differencing filter on the accumulated sediment series $S_c(t)$, i.e., equation (8) with the generic function $X(t)$ replaced now by $S_c(t)$ and using as differencing filters wavelets of increasing order $g_N(t)$, where $N = 2, 3$, and 4. It is noted that by using the third derivative of the Gaussian, $g_3(t)$, on the accumulated sediment series gives fluctuations that represent second-order increments of the bed load transport rates; that is, they capture the local rate of change in the sediment transport rates. This filtering guarantees removal of linear trends in the rate of sediment transport series, which, if present, can influence the results. Indeed such rate changes were found present during the 20 h duration of our data collection [see *Fienberg et al.*, 2008, Figure 3] and thus the $g_3(t)$ was adopted for our analysis. However, it is noted that the use of lower-order wavelets does not significantly change the estimates of the parameters as can be seen from the detailed Table 2. Having defined the fluctuations, the statistical moments $M(q, a)$ were then computed (equation (5)), and are shown as a function of scale in Figure 5, for pan 3 (see Figure 1). Similar results were obtained for the other pans, except for pans 1 and 5 which suffered from wall effects and showed no good scaling range. Three different regimes can be distinguished for both the low and high discharge: a small-scale regime (scales below 1 min) which is judged to be noise dominated (see section 2.1); a log-log linear

scaling regime in the temporal range of approximately 1 to 10 min; and then a short transitional regime before a leveling off of the moments is reached. Here we focus on the longer scaling regime between 1 min and 10 min marked by the dashed lines in Figure 5. The scaling exponents of the various moment orders, $\tau(q)$, were estimated using linear regression within this scaling range and are shown for both discharges in Figure 5 (bottom). It can be seen that both curves deviate from linear behavior and hence depart from simple scaling and instead demonstrate multiscaling. The parameters c_1 and c_2 found by fitting the quadratic model (equation (13)) to these curves are presented in Table 3, along with a summary of the scaling range and parameters for the other pans for which uninterrupted data were available. It is noted that the quadratic fit is very good and the fitted curves are indistinguishable from the measured points.

[33] This scaling of the moments reflects the scaling of the pdf of sediment fluctuations. Figure 6 shows the pdf's of the sediment transport rates (defined as accumulations over an interval divided by the length of that interval) for 2-min and 10-min intervals for both high and low discharge. It can be seen that for both flow conditions, the very skewed and fat-tailed pdf at 2 min changes to a much more symmetrical pdf at 10 min, although in the case of the low flow, there is still some skewness present even at the larger sampling time. It is recalled that the parameters c_1 and c_2 control this pdf change over scales through the rescaling kernel (equation (12)). An easy way to observe the relative narrowing of the pdf with increasing scale is via the coefficient of variation C_v computed from the data, which is plotted in Figure 7 as a function of scale. The decreasing values of C_v with increasing scale show that the width (spread) of the pdf changes with scale in a different manner compared to the mean (it reduces more quickly), in agreement with earlier observations by *Kuhnle and Southard* [1988], and hence reinforces the conclusion that sediment transport fluctuations exhibit multiscaling. A monoscaling function would have constant C_v as mean and standard deviation would rescale similarly (see equation (6)).

[34] Concentrating on the first-order ($q = 1$) statistical moment, which is the mean sediment accumulation in an interval Δt (scale a in the previous notation), we note that it scales as $\Delta t^{\tau(1)}$ where $\tau(1) = c_1 - c_2/2$ from equation (13). Using the values of c_1 and c_2 (Table 3) for low flows, it implies that within the scaling range of 1 and 10 min the mean amount of accumulated sediment ($\langle S(t, \Delta t) \rangle$) increases as approximately $\sqrt{\Delta t}$. If one doubles the sampling interval, for example, the amount of sediment accumulated does not double but increases only by a factor of about 1.41. When considering the mean sediment transport rate, ($\langle S(t, \Delta t)/\Delta t \rangle$), the above results imply that it scales as $(\Delta t)^{-0.5}$ or that the bed load transport rate decreases with increasing sampling interval Δt . In other words, doubling the sampling interval results in a transport rate that is approximately 0.7 ($= 1/\sqrt{2}$) times smaller.

[35] For high flow rates, the estimated value of $\tau(1)$ is approximately 1.1 (using the values of c_1 and c_2 from Table 3 in equation (13)) implying that within the scaling range of 1 and 10 min, the mean amount of accumulated sediment increases as approximately $(\Delta t)^{1.1}$. In this case, doubling the sampling interval increases accumulated sediment by a

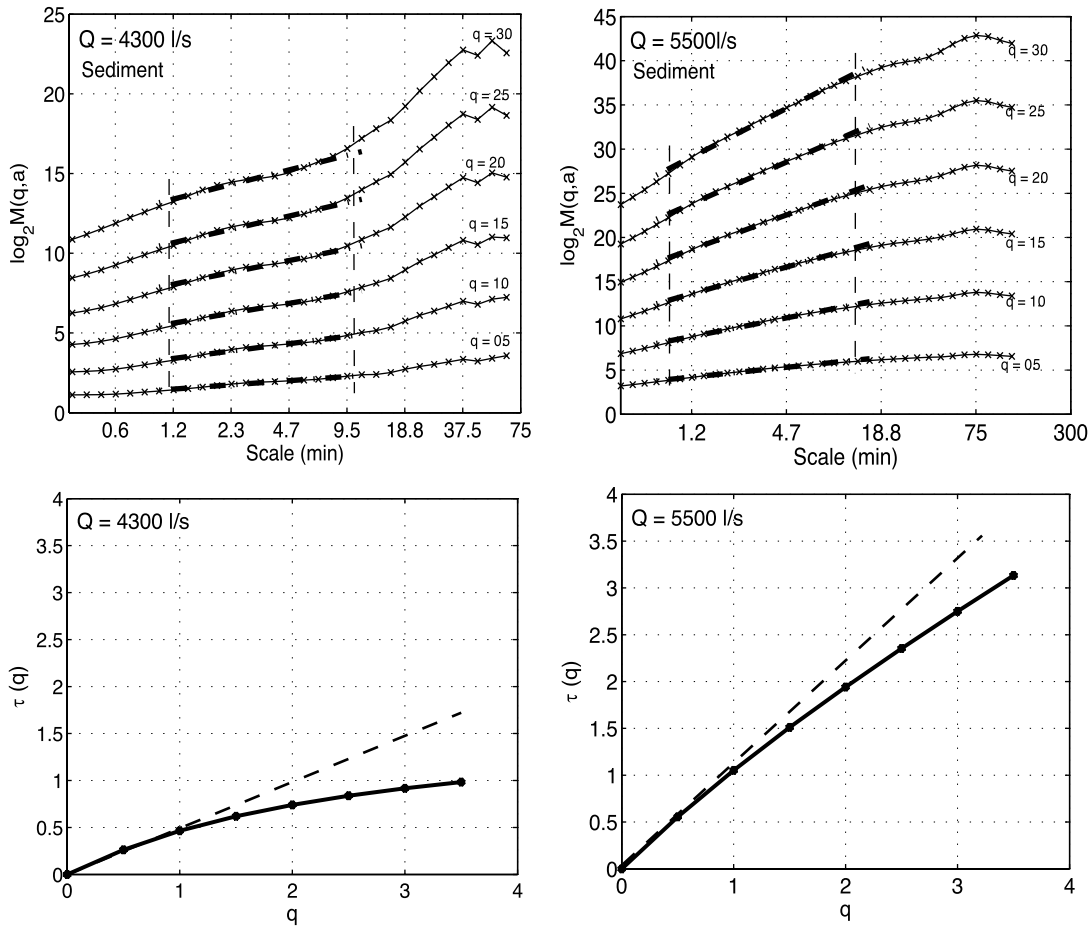


Figure 5. (top) Statistical moments of the fluctuations of the sediment transport series as a function of scale and (bottom) the scaling exponents $\tau(q)$ estimated from the log-log linear regressions within the scaling regions. Notice the deviation of $\tau(q)$ from the linear line establishing the presence of multifractality. (left) For low-transport conditions and (right) for high-transport conditions.

factor of about 2.1. Considering the mean sediment transport rate, one sees that in the high-flow conditions the rate does not remain constant with sampling interval (within the range of sampling interval of 1 to 10 min) but rather slightly increases by a factor of approximately 1.1 ($= 2^{0.10}$).

[36] The above scaling applies only to the mean and is controlled by the value of $(c_1 - c_2/2)$. As discussed in sections 3.2 and 3.4, our analysis allows one to quantify how higher-order statistical moments change with sampling interval in a similar way, for example the second moment about the origin changes as a power law on scale with an exponent $2(c_1 - c_2)$, etc., as dictated by equations (6) and (13).

[37] Turning to the singularity spectrum $D(h)$ which characterizes more directly the abrupt fluctuations of the sediment transport series, we recall that it can be computed from the scaling exponents $\tau(q)$ via the Legendre transform (equation (7) or directly from equation (14) using the fitted parameters c_1 and c_2). Figure 8a shows the $D(h)$ spectrum for the sediment transport in pan 3, calculated from the quadratic model fit using the parameters in Table 3. It can be seen that at the low discharge, the sediment transport series is both rougher on the average and more intermittent

(lower c_1 and higher c_2 , respectively). Conversely, the high-discharge case results in a much smoother and less intermittent sediment transport series (higher c_1 and lower c_2 , respectively). As it can be seen from Figure 8a, for low flow rates, h_{\min} is approximately zero, and h_{\max} is slightly larger than 1. This implies that there are clustered regions in the sediment transport rate series where very high fluctuations are expected over very small intervals (a value of $h = 0$ corresponds to a discontinuous signal) while there are also

Table 3. Summary of Statistical Scaling Analysis Results for the Bed Load Sediment Series^a

Pan	Scaling Range (min)	Shields Stress	$\tau(2) - 2\tau(1)$	c_1	c_2
$Q = 4300$ L/s					
2	1.2–10		-0.20	0.56	0.14
3	1.2–10	0.085	-0.19	0.49	0.13
4	1–8		-0.15	0.47	0.10
$Q = 5500$ L/s					
2	1–10		-0.13	1.07	0.09
3	1–10	0.196	-0.16	1.07	0.10
4	1–10		-0.15	1.12	0.11

^aSee text for definition of variables.

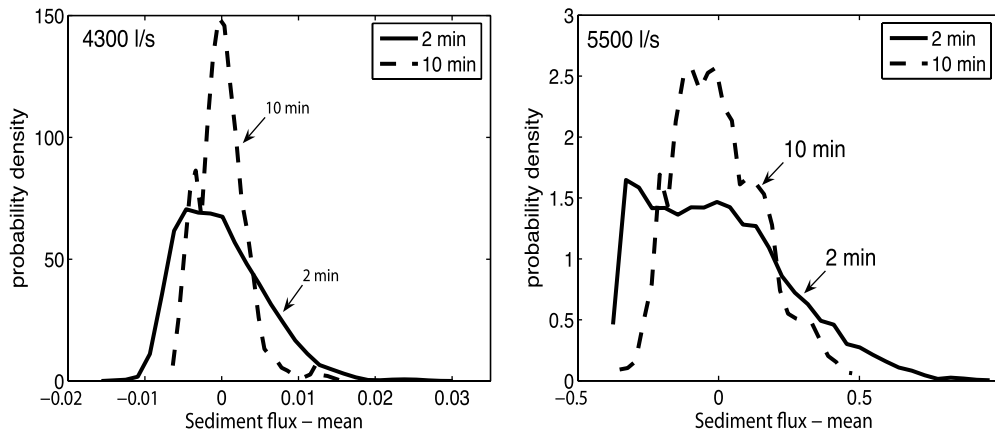


Figure 6. Probability distribution functions of the sediment transport rate (flux) for sampling intervals of 2 and 10 min for (left) low- and (right) high-discharge rates. The probability distributions have been shifted to zero mean for comparison.

regions that are very smooth (a value of $h = 1$ corresponds to a signal with continuous first derivative). For high flow rates the values of h_{\min} and h_{\max} are approximately 0.8 and 1.5, implying that the sediment transport series is very smooth overall but there are limited clustered regions where some abrupt fluctuations at small scales are encountered (signal slightly nondifferentiable as $h < 1$) while the majority of the series is very smooth. One would expect that these bursts in the sediment transport series are connected to high fluctuations in the bed elevation series which would allow to a lesser or larger degree a collective mobilization of gravel particles. In section 4.2 a multifractal analysis to characterize the roughness and intermittency of bed elevation fluctuations is presented.

4.2. Bed Elevation Scaling

[38] Spatial bed elevation fluctuations have been previously analyzed in terms of their scaling properties, and deviation from simple scaling has been reported [Nikora and Walsh, 2004]. Here the temporal fluctuations of bed elevation were analyzed with the wavelet-based multiscale framework, and scaling of the moments was documented within the range of scales from approximately 1 to 10 min (see Figure 9), which coincides with the scaling range observed in the sediment transport series and suggests a close link between the dynamics of the two series. Above the characteristic scale of 10 min, the moments leveled off and the statistical quantities became independent of time scale. The scaling exponents $\tau(q)$ for these moments are shown in Figure 9, for the high- and low-discharge experiments. As other authors have reported [e.g., see Nikora and Walsh, 2004], a deviation from simple scaling is observed for both discharge rates indicating the presence of temporal heterogeneity in the local roughness (what we have called “intermittency”) in bed elevation fluctuations. The parameters c_1 and c_2 fitted to the $\tau(q)$ curves of the bed elevation fluctuation series are displayed in Table 4, and the corresponding singularity spectra $D(h)$ are presented in Figure 8b. Similar to the sediment transport fluctuations, we observe that bed elevation fluctuations are rougher on an average in the low-discharge case than in the high-discharge case ($c_1 = 0.57$ versus $c_1 = 0.68$), although to a lesser extent

than in the sediment series. However, considering the degree of intermittency in the bed elevation fluctuations, we see that it is higher at the high-transport case (a wider $D(h)$ spectrum and a larger c_2 value) with a coefficient of intermittency $c_2 = 0.13$, versus a narrower $D(h)$ and $c_2 = 0.06$ in the case of low transport. This is reverse from what is observed in the sediment transport fluctuations (see also Figure 8a) and calls for an explanation based on further experimentation and mechanistic modeling.

5. Discussion

[39] The simultaneous collection of bed load transport and bed elevation data in a field-scale channel is the major strength of the experimental setup used in this work. The large channel geometry, and high temporal resolution of the data, allowed robust statistical analysis over a wide range of temporal scales. Despite the more comprehensive data sets collected as part of the StreamLab06 experiments our analysis here is concentrated on two data sets at two different flow rates, as these are the only data currently

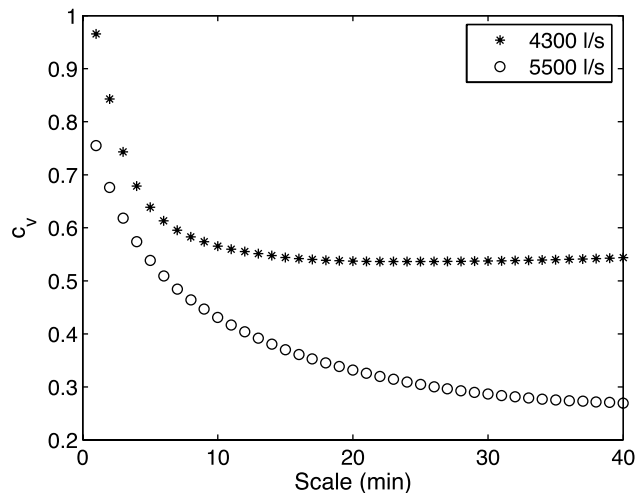


Figure 7. Coefficient of variation of the bed load sediment transport series.

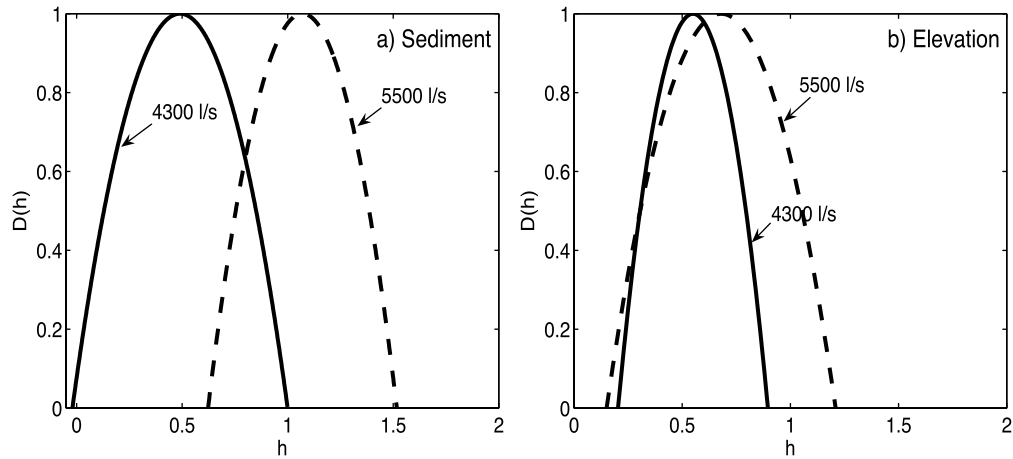


Figure 8. Fitted quadratic singularity spectra $D(h)$ obtained for (a) bed load sediment transport series and (b) bed elevation fluctuation series for the low- and high-discharge cases, respectively.

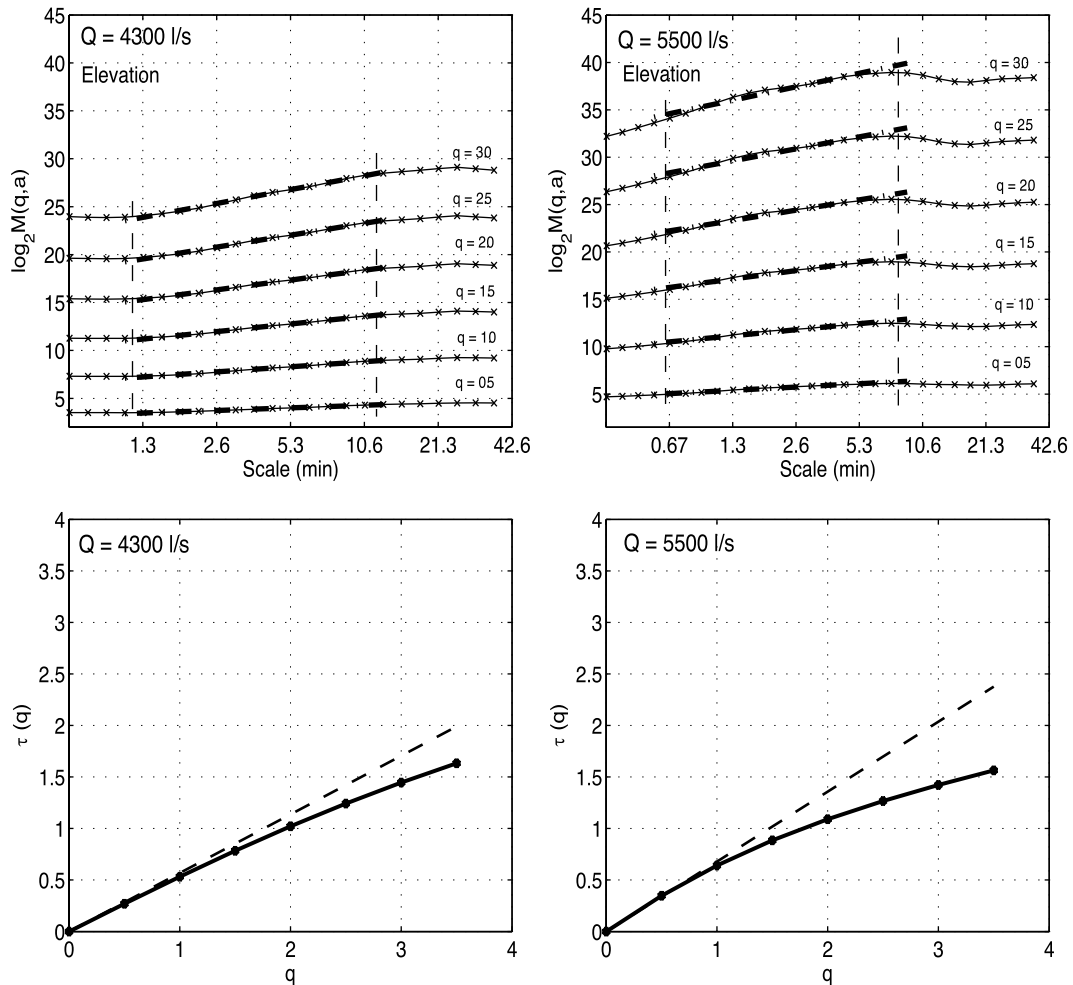


Figure 9. (top) Statistical moments of the fluctuations of the bed elevation time series as a function of scale and (bottom) the scaling exponents $\tau(q)$ estimated from the log-log linear regressions within the scaling regions. Notice the deviation of $\tau(q)$ from the linear line establishing the presence of multifractality. (left) For low-transport conditions and (right) for high-transport conditions.

Table 4. Summary of Statistical Scaling Analysis Results for the Bed Elevation Time Series^a

Probe	Scaling Range (min)	Shields Stress	$\tau(2) - 2\tau(1)$	c_1	c_2
$Q = 4300 \text{ L/s}$					
4	1-10	0.085	-0.04	0.57	0.06
5	1-10		-0.06	0.53	0.08
$Q = 5500 \text{ L/s}$					
2	0.5-8		-0.18	0.65	0.12
3	0.5-8	0.196	-0.19	0.68	0.14
4	0.5-8		-0.20	0.76	0.13

^aSee text for definition of variables.

available for analysis. The mixed grain size distribution of the feed material, while beneficial for mimicking a natural gravel stream, makes it more difficult to discern the influences of spatial grain size sorting [Iseya and Ikeda, 1987; Kuhnle and Southard, 1988; Cudden and Hoey, 2003; Frey et al., 2003] from those of bed topography and collective grain motion [Gomez et al., 1989; Jerolmack and Mohrig, 2005; Ancey et al., 2008] on sediment transport fluctuations. Also, for this experiment we do not have any data regarding armoring of the streambed over the duration of the experiments, or the grain size distributions of individual sediment pulses. With these limitations in mind, in this section we place our experimental results and analysis in the context of laboratory and field studies of sediment transport fluctuations in uniform and mixed grain size channels.

[40] The multiscaling analysis demonstrates how the statistical moments of bed load transport rate depend on the time scale of observation. To illustrate, we first examine the behavior of the mean transport rate (the first moment). Estimating mean sediment transport rate is essential for measuring the material flux through a river, and for model input and/or calibration. For the low-discharge run ($\tau^*_b = 0.085$), mean transport rate decreased with sampling interval, while at higher discharge ($\tau^*_b = 0.196$), the trend reversed: mean transport rate slightly increased with sampling interval over a comparable time range. A similar trend was discovered by Bunte and Abt [2005], who studied the effect of sampling interval on bed load transport rates measured using Helley-Smith samplers deployed in a mixed gravel-cobble stream of a size comparable to our experiments. They found that in moderate to high flows (50% bankfull to almost bankfull conditions), 2 min sampling led to an average transport rate 2 to 5 times lower than that found with 10 min sampling. However, at lower flows (close to the incipient gravel motion), 2 min sampling overestimated the transport rates at 10 min sampling by a factor of almost 3. Although not directly comparable, the trends observed are qualitatively the same as our experiments (Figure 10). Bunte and Abt [2005] attribute the higher-discharge trend to the effect of large but infrequent transport events associated with the crests of bed forms: small sampling intervals underestimate mean transport because they are likely to miss these events. They suggest that the reversal in trend for the low-discharge observations is the result of sampling and computational difficulties, rather than a “real” effect. Our high-resolution experiments demonstrate that this trend reversal might in fact be real.

[41] It is stressed that it is difficult to quantitatively compare the field results to our laboratory experiments, due to differences in transport and lack of the detailed field

data. Bunte and Abt [2005] do not report Shields stress, but they report that their low-flow observations correspond to incipient sediment motion which is supported by our calculation of their critical Shields stress ($\tau^* = 0.047$) using their reported bankfull flow characteristics. Our low-flow experiment had a Shields stress almost twice the critical value, making it comparable in terms of stress to their moderate flow observations. Thus it seems that in both the study of Bunte and Abt and our study, suggest a reversal in trend, from decreasing to increasing mean transport rate with sampling interval, as bed stress increases. The fact that the reversal appears to occur for different stress values in the

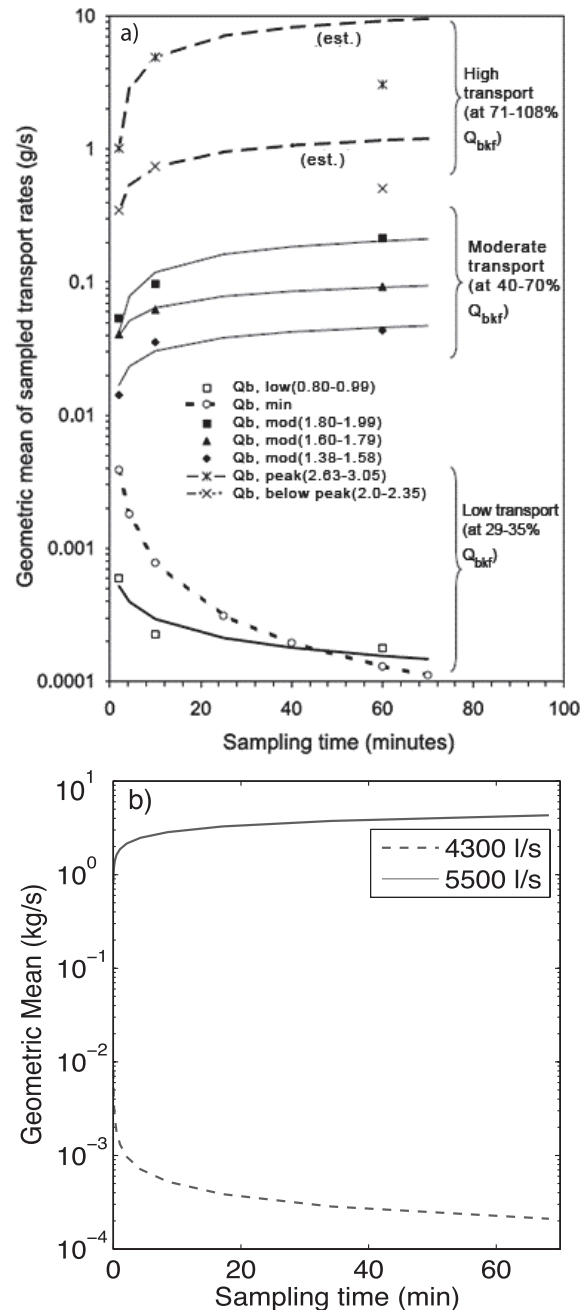


Figure 10. Geometric means at different sampling times from (a) field experiments (reproduced from Bunte and Abt [2005]) and (b) theoretical results from this study.

field and the laboratory may be the result of the multiple intricacies of sediment transport and grain size sorting of heterogeneous mixtures in turbulent flows. Clearly, experiments systematically document how the statistics of transport rate change with bed stress over a wide range of values would be helpful in illuminating this point.

[42] Several field and laboratory experiments have documented sediment transport fluctuations in mixed grain size sediments. *Iseya and Ikeda* [1987] found strong longitudinal grain size sorting in mixed gravel and sand experiments, which caused periodic fluctuations in transport rate due to changing local sediment supply. Such periodic pulses in gravel-sand mixtures have also been reported by *Kuhnle and Southard* [1988] and *Frey et al.* [2003]. These experiments cannot be directly compared to our results, however, because they had limited bed topography and/or antidunes, while our experimental channel allowed for the growth of large bed forms in subcritical flow. These studies suggest that the creation and destruction of sediment patches of different grain sizes [see also *Cudden and Hoey*, 2003] due to longitudinal grain size sorting within the channel likely contributed somewhat to the observed transport fluctuations in our experiments, but are not capable of explaining all of this variability.

[43] Sediment transport rates became smoother and less intermittent with increasing bed stress in our experiments, in agreement with previous observations. Near the threshold of motion, grains are in partial transport because local bed stress fluctuates above and below the threshold value. These turbulent fluctuations, along with grain-to-grain interactions at the bed, result in intermittent and collective motion of grains, leading to nonrandom transport rate fluctuations with heavy tails [*Ancey et al.*, 2008]. In a mixed grain size bed, size selective transport often occurs which may enhance this effect [*Kuhnle and Southard*, 1988]. The experiments of *Ancey et al.* [2008] demonstrate that such fluctuations can occur even in glass spheres of uniform size, with little or no bed topography. As bed stress is increased such that the local stress fluctuations are always above the critical value, all grains become entrained in the flow as the intermittent, collective motions of grains gives way to continuous transport [*Iseya and Ikeda*, 1987; *Kuhnle and Southard*, 1988; *Ancey et al.*, 2008; *Strom et al.*, 2004]. While this effect has been documented qualitatively by previous authors, our results quantify these changes in the statistics of sediment fluctuations with bed shear stress.

[44] Bed elevation also became smoother with increasing transport, meaning that the magnitude of high-frequency fluctuations at small scales was reduced overall. At low-flow conditions, topographic fluctuations were of the order of the grain scale (Figure 3), supporting the idea that grain-grain interactions (and perhaps longitudinal grain size sorting) dominated transport fluctuations as described above. With increasing bed stress, and presumably full mobility of all grains in transport based on Shields stress calculations, the bed organized into large-scale bed forms (Figure 4). Data indicate that higher-frequency (smaller-scale) topography, likely representing clusters of grains, became less prevalent at higher flows where bed topography was dominated by dune forms. Interestingly, although the bed became smoother overall from low to high discharge, intermittency increased. In other words, high small-scale

frequency fluctuations in bed topography became less prevalent overall, but also less uniformly distributed. This may be due to irregular clusters of grains superimposed on larger scale, more regular dune features. However, observations of grains on the bed were not made and so these ideas remain speculative at this stage. Our experiments highlight the need to simultaneously document bed topography, bed load transport rates and individual particle motions (e.g., as those of *Schmeeckle et al.* [2001], *Papanicolaou et al.* [2002], and *Ancey et al.* [2006]) in order to further our understanding of what contributes to transport fluctuations at the smallest to largest scales.

[45] The scaling ranges of both transport rates and bed elevation series are similar with a leveling off, or saturation, at approximately the same time scales, indicating that fluctuations in transport are intimately related to bed topography. While the nature of these dependencies is still unclear, a practical result may be obtained. The scale-dependent nature of transport (within 1 and 10 min in this study) means that measured rates at different time intervals are not directly comparable. In our experiments, both transport and bed elevation exhibit no time dependence when measured over intervals greater than 10 to 15 min. In other words, if we measure for a period of time that is larger than the time scale associated with the migration of the largest topographic feature, we can obtain mean values for bed topography and transport rate that have no time dependence [*Fienberg et al.*, 2008]. From a practical point of view, this is the mean transport rate one should try to obtain in the field. Measurements of bed topography from a river could be used to determine the upper scaling limit of fluctuations, which determines the time scale over which one should deploy a sampler to obtain a representative “mean” bed load transport value. As discussed by *Fienberg et al.* [2008], this approach is possible in flumes and small streams where the time scale is of the order of tens of minutes. Since the size of bed forms scales with river depth, however, this approach quickly becomes impractical as river size increases: deployment of bed load samplers for long durations can result in overfilling and clogging [e.g., *Bunte and Abt*, 2005], or integrating over changing flow conditions. In this case, determining the scale-dependent nature of transport rate becomes critical.

6. Conclusions

[46] In this paper we introduce a formalism, typically used in turbulence studies, to quantify two properties in sediment transport and concurrent bed elevation series: the “average roughness” of the series (depicting the average strength of local abrupt fluctuations in the signal) and the “intermittency” (depicting the temporal heterogeneity of fluctuations of different strength). In the bed load sediment transport rates, we documented the presence of a rougher and more intermittent behavior at low-transport conditions (dimensionless bed shear stress of about twice the critical value) transiting to a smoother and less intermittent behavior at high-transport conditions (dimensionless shear stress of about five times the critical value).

[47] Apart from simply quantifying roughness and intermittency of the sediment transport rates, the results of our analysis provide a framework for quantifying how the

probability distribution of sediment transport rates changes with sampling interval and thus have important practical implications. (It is interesting to note that the change of pdf with scale is parameterized in terms of the roughness and intermittency parameters which characterize the burstiness of the series.) Specifically, our analysis demonstrated that the statistics of bed load sediment transport rates depend strongly on scale (sampling interval) and this dependence varies with the discharge conditions. Our results agree with the field observations reported by *Bunte and Abt* [2005] for mean bed load rates and call for a more systematic study to precisely quantify this scale dependence in terms of grain size sorting and bed shear stress. It is noted that the theoretical framework we propose here offers the ability to go beyond the mean and compare the whole probability density function, including extreme values or quantiles, at different scales. This is important for example when the pdf of sediment transport rates has been estimated from data at one particular sampling interval and an extreme exceedance quantile (say, relevant to an ecological smaller-scale functional disturbance) needs to be estimated. Our methodology can bridge this gap in scales and also provide a framework with which comparison of sediment rates sampled with different instruments can be made.

[48] A problem of continuous interest in the literature is the relation of microscale (particle-scale) dynamics to the macroscale behavior of sediment transport [e.g., *Drake et al.*, 1988; *Papanicolaou et al.*, 2002; *Schmeeckle et al.*, 2001; *Schmeeckle and Nelson*, 2003; *Ancey et al.*, 2006, 2008]. Although not precisely quantified in this paper, it is worth noting that the multiscale statistical behavior of sediment transport rates (as quantified here via the signal roughness and intermittency) seems consistent with known particle-scale dynamics. For example, at low flows, a rougher but more temporally homogeneous (less intermittent) bed elevation series was documented, indicative of the dominance of high-frequency localized grain clusters; this bed microtopography apparently gave rise to sediment transport rates that are almost of equal roughness but are more inhomogeneous in time (more intermittent) (see Figure 8). This might be due to the collective motion of grains responding to local bed stress fluctuating above and below the critical value. It appears that as bed stress increased, grain patches became less prevalent and more irregular (roughness in bed elevations decreased but intermittency increased) as the bed organized into large-scale dunes, and bed load transport became smoother and more homogeneous in time as entrainment of all grains commenced. This speaks for the collective or cooperative behavior of particle movement that has different dynamics at low and high flows and depends on the presence or absence of self-formed structures on the bed [e.g., *Drake et al.*, 1988; *Ancey et al.*, 2008].

[49] We see our study as a first step in the direction of understanding the scale dependency of sediment transport rates over the continuum of flow discharge conditions and grain size distributions and relating the statistics of bed elevations to the statistics of bed load sediment transport. More controlled experiments have to be performed and analyzed with different particle sizes (from a single particle size to a broad particle size distribution and for gravel and sand beds) and a spectrum of discharge rates, to fully characterize the intermittency of bed load sediment trans-

port rates and how it relates to that of the bed elevation fluctuations, and (eventually) to particle size dynamics. Also, the documented statistical structure of sediment transport rates can be seen as providing an additional model diagnostic that mechanistic models should be able to reproduce, and as such, it is interesting to ask as to whether any known sediment transport model can reproduce the multiscale characteristics reported in this study.

[50] **Acknowledgments.** This research was inspired by the StreamLab06 experiments conducted at St. Anthony Falls Laboratory as part of an interdisciplinary research agenda set by the National Center for Earth-surface Dynamics (NCED) at the University of Minnesota. NCED is a Science and Technology Center funded by NSF's Office of Integrative Activities under agreement EAR-0120914. We thank Christophe Ancey, Thanos Papanicolaou, and an anonymous reviewer, as well as the Associate Editor and Michael Church, whose suggestions and constructive comments substantially improved our presentation and refined our interpretations. We also thank Peter Wilcock, Gary Parker, and Mark Schmeeckle for stimulating discussions. All computational resources were kindly provided by the Minnesota Supercomputing Institute. The senior author acknowledges support from the Joseph T. and Rose S. Ling Professorship in Environmental Engineering at the University of Minnesota. The StreamLab06 data are available from the authors upon request.

References

- Aberle, J., and V. Nikora (2006), Statistical properties of armored gravel bed surfaces, *Water Resour. Res.*, *42*, W11414, doi:10.1029/2005WR004674.
- Ancey, C., T. Böhm, M. Jodeau, and P. Frey (2006), Statistical description of sediment transport experiments, *Phys. Rev. E*, *74*(1), 011302, doi:10.1103/PhysRevE.74.011302.
- Ancey, C., A. C. Davidson, T. Böhm, M. Jodeau, and P. Frey (2008), Entrainment and motion of coarse particles in a shallow water stream down a steep slope, *J. Fluid Mech.*, *595*, 83–114, doi:10.1017/S0022112007008774.
- Arneodo, A., E. Bacry, and J. F. Muzy (1995), The thermodynamics of fractals revisited with wavelets, *Physica A*, *213*, 232–275, doi:10.1016/0378-4371(94)00163-N.
- Arneodo, A., J. F. Muzy, and S. G. Roux (1997), Experimental analysis of self-similarity and random cascade processes: Application to fully developed turbulence data, *J. Phys. II*, *7*(2), 363–370, doi:10.1051/jp2:1997130.
- Arneodo, A., N. Decoster, and S. G. Roux (1999a), Intermittency, lognormal statistics, and multifractal cascade process in high-resolution satellite images of cloud structure, *Phys. Rev. Lett.*, *83*(6), 1255–1258, doi:10.1103/PhysRevLett.83.1255.
- Arneodo, A., S. Manneville, J. F. Muzy, and S. G. Roux (1999b), Revealing a lognormal cascading process in turbulent velocity statistics with wavelet analysis, *Philos. Trans. R. Soc., Ser. A*, *357*(1760), 2415–2438.
- Bunte, K., and S. R. Abt (2005), Effect of sampling time on measured gravel bed load transport rates in a coarse-bedded stream, *Water Resour. Res.*, *41*, W11405, doi:10.1029/2004WR003880.
- Castaing, B., Y. Gagne, and E. J. Hopfinger (1990), Velocity probability density-functions of high Reynolds-number turbulence, *Physica D*, *46*, 177–200, doi:10.1016/0167-2789(90)90035-N.
- Cudden, J. R., and T. B. Hoey (2003), The causes of bedload pulses in a gravel channel: The implications of bedload grain-size distributions, *Earth Surf. Processes Landforms*, *28*, 1411–1428, doi:10.1002/esp.521.
- Delour, J., J. Muzy, and A. Arneodo (2001), Intermittency of 1D velocity spatial profiles in turbulence: A magnitude cumulant analysis, *Eur. Phys. J. B*, *23*, 243–248, doi:10.1007/s100510170074.
- Dinehart, R. L. (1992), Evolution of coarse gravel bed forms: Field measurements at flood stage, *Water Resour. Res.*, *28*(10), 2667–2689, doi:10.1029/92WR01357.
- Drake, T., R. Shreve, W. Dietrich, P. Whiting, and L. Leopold (1988), Bedload transport of fine gravel observed by motion-picture photography, *J. Fluid Mech.*, *192*, 193–217, doi:10.1017/S0022112088001831.
- Fienberg, K., A. Singh, D. Jerolmack, J. Marr, and E. Foufoula-Georgiou (2008), A theoretical framework for interpreting and quantifying the sampling time dependence of gravel bedload transport rates, paper presented at Bedload Research International Cooperative Meeting, Minneapolis, Minn., 11–14 April.
- Foufoula-Georgiou, E., and V. Sapozhnikov (1998), Anisotropic scaling in braided rivers: An integrated theoretical framework and results from application to an experimental river, *Water Resour. Res.*, *34*(4), 863–867, doi:10.1029/98WR00216.

- Frey, P., C. Ducotet, and J. Jay (2003), Fluctuations of bed load solid discharge and grain size distribution on steep slopes with image analysis, *Exp. Fluids*, *35*, 589–597, doi:10.1007/s00348-003-0707-9.
- Frisch, U. (1995), *Turbulence: The Legacy of A. N. Kolmogorov*, Cambridge Univ. Press, New York.
- Gangodagamage, C., E. Barnes, and E. Fofoula-Georgiou (2007), Scaling in river corridor widths depicts organization in valley morphology, *J. Geomorphol.*, *91*, 198–215, doi:10.1016/j.geomorph.2007.04.014.
- Gomez, B., R. L. Naff, and D. W. Hubbell (1989), Temporal variation in bedload transport rates associated with the migration of bedforms, *Earth Surf. Processes Landforms*, *14*, 135–156, doi:10.1002/esp.3290140205.
- Gupta, V., and E. Waymire (1996), Multiplicative cascades and spatial variability in rainfall, river networks, and floods, in *Reduction and Predictability of Natural Disasters, Proc. Vol. Santa Fe Inst. Stud. Sci. Complexity*, vol. 25, edited by J. B. Rundle, D. L. Turcotte, and W. Klein, Addison-Wesley, Boston, Mass.
- Iseya, F., and H. Ikeda (1987), Pulsations in bedload transport rates induced by a longitudinal sediment sorting: A flume study using sand and gravel mixtures, *Geogr. Ann., Ser. A*, *69*, 15–27, doi:10.2307/521363.
- Jaffard, S. (1997), Multifractal formalism for functions, *SIAM J. Math. Anal.*, *28*(4), 944–998, doi:10.1137/S0036141095282991.
- Jerolmack, D. J., and D. Mohrig (2005), A unified model for subaqueous bed form dynamics, *Water Resour. Res.*, *41*, W12421, doi:10.1029/2005WR004329.
- Jerolmack, D. J., and P. M. Sadler (2007), Transience and persistence in the depositional record of continental margins, *J. Geophys. Res.*, *112*, F03S13, doi:10.1029/2006JF000555.
- Kuhnle, R. A., and J. B. Southard (1988), Bed load fluctuations in a gravel bed laboratory channel, *Water Resour. Res.*, *24*(2), 247–260, doi:10.1029/WR024i002p00247.
- Kumar, P., and E. Fofoula-Georgiou (1997), Wavelet analysis for geophysical applications, *Rev. Geophys.*, *35*(4), 385–412, doi:10.1029/97RG00427.
- Lashermes, B., and E. Fofoula-Georgiou (2007), Area and width functions of river networks: New results on multifractal properties, *Water Resour. Res.*, *43*, W09405, doi:10.1029/2006WR005329.
- Lashermes, B., E. Fofoula-Georgiou, and W. E. Dietrich (2007), Channel network extraction from high resolution topography data using wavelets, *Geophys. Res. Lett.*, *34*, L23S04, doi:10.1029/2007GL031140.
- Lovejoy, S., and D. Schertzer (1985), Generalized scale invariance and fractal models of rain, *Water Resour. Res.*, *21*(8), 1233–1250, doi:10.1029/WR021i008p01233.
- Lovejoy, S., D. Schertzer, P. Silas, Y. Tessier, and D. Lavallée (1993), The unified scaling model of atmospheric dynamics and systematic analysis in cloud radiances, *Ann. Geophys.*, *11*, 119–127.
- Mallat, S. (1998), *A Wavelet Tour in Signal Processing*, Academic, San Diego, Calif.
- Marani, M., A. Rinaldo, R. Rigon, and I. Rodriguez-Iturbe (1994), Geomorphological width functions and the random cascade, *Geophys. Res. Lett.*, *21*, 2123–2126, doi:10.1029/94GL01933.
- Meyer-Peter, E., and R. Müller (1948), Formulas for bed-load transport, paper presented at 2nd Congress, Int. Assoc. of Hydraul. Res., Stockholm.
- Muzy, J. F., E. Bacry, and A. Arneodo (1994), The multifractal formalism revisited with wavelets, *Int. J. Bifurcat. Chaos*, *4*, 245–302, doi:10.1142/S0218127494000204.
- Nikora, V., and D. M. Hicks (1997), Scaling relationships for sand wave development in unidirectional flows, *J. Hydraul. Eng.*, *123*, 1152–1156, doi:10.1061/(ASCE)0733-9429(1997)123:12(1152).
- Nikora, V., and J. Walsh (2004), Water-worked gravel surfaces: High-order structure functions at the particle scale, *Water Resour. Res.*, *40*, W12601, doi:10.1029/2004WR003346.
- Nikora, V., A. N. Sukhodolov, and P. M. Rowinski (1997), Statistical sand wave dynamics in one-directional water flows, *J. Fluid Mech.*, *351*, 17–39, doi:10.1017/S0022112097006708.
- Nikora, V., H. Habersack, T. Huber, and I. McEwan (2002), On bed particle diffusion in gravel bed flows under weak bed load transport, *Water Resour. Res.*, *38*(6), 1081, doi:10.1029/2001WR000513.
- Papanicolaou, A., P. Diplas, N. Evangelopoulos, and S. Fotopoulos (2002), Stochastic incipient motion criterion for spheres under various bed packing conditions, *J. Hydraul. Eng.*, *128*, 369–380, doi:10.1061/(ASCE)0733-9429(2002)128:4(369).
- Parisi, G., and U. Frisch (1985), On the singularity structure of fully developed turbulence, in *Turbulence and Predictability in Geophysical Fluid Dynamics*, edited by M. Ghil et al., pp. 84–87, North-Holland, Amsterdam.
- Rinaldo, A., I. Rodriguez-Iturbe, R. Rigon, E. Ijjasz-Vasquez, and R. Bras (1993), Self-organized fractal river networks, *Phys. Rev. Lett.*, *70*, 822–825, doi:10.1103/PhysRevLett.70.822.
- Sadler, P. M. (1981), Sediment accumulation and the completeness of stratigraphic sections, *J. Geol.*, *89*, 569–584.
- Sadler, P. M. (1999), The influence of hiatuses on sediment accumulation rates, *GeoRes. Forum*, *5*, 15–40.
- Schmeeckle, M. W., and J. M. Nelson (2003), Direct numerical simulation of bedload transport using a local, dynamic boundary condition, *Sedimentology*, *50*(2), 279–301, doi:10.1046/j.1365-3091.2003.00555.x.
- Schmeeckle, M. W., J. M. Nelson, J. Pitlick, and J. P. Bennett (2001), Interparticle collision of natural sediment grains in water, *Water Resour. Res.*, *37*(9), 2377–2391, doi:10.1029/2001WR000531.
- Schroeder, M. (1991), *Fractals, Chaos, Power Laws: Minutes from an Infinite Paradise*, W. H. Freeman, New York.
- Strom, K., A. N. Papanicolaou, N. Evangelopoulos, and M. Odeh (2004), Microforms in gravel bed rivers: Formation, disintegration, and effects on bedload transport, *J. Hydraul. Eng.*, *130*, 554–567, doi:10.1061/(ASCE)0733-9429(2004)130:6(554).
- Sumer, B. M., L. H. C. Chua, N. S. Cheng, and J. Fredsoe (2003), Influence of turbulence on bed load sediment transport, *J. Hydraul. Eng.*, *129*, 585–596, doi:10.1061/(ASCE)0733-9429(2003)129:8(585).
- Turcotte, D. L. (1997), *Fractals and Chaos in Geology and Geophysics*, 2nd ed., Cambridge Univ. Press, New York.
- Venugopal, V., S. G. Roux, E. Fofoula-Georgiou, and A. Arneodo (2006a), Revisiting multifractality of high-resolution temporal rainfall using a wavelet-based formalism, *Water Resour. Res.*, *42*, W06D14, doi:10.1029/2005WR004489.
- Venugopal, V., S. G. Roux, E. Fofoula-Georgiou, and A. Arneodo (2006b), Scaling behavior of high resolution temporal rainfall: New insights from a wavelet-based cumulant analysis, *Phys. Lett. A*, *348*, 335–345, doi:10.1016/j.physleta.2005.08.064.
- Wilcock, P. R., C. H. Orr, and J. D. G. Marr (2008), The need for full-scale experiments in river science, *Eos Trans. AGU*, *89*(1), doi:10.1029/2008EO010003.
- Yarnell, S. M., J. F. Mount, and E. W. Larsen (2006), The Influence of relative sediment supply on riverine habitat heterogeneity, *Geomorphology*, *80*, 310–324, doi:10.1016/j.geomorph.2006.03.005.

K. Fienberg, E. Fofoula-Georgiou, J. Marr, and A. Singh, St. Anthony Falls Laboratory, University of Minnesota-Twin Cities, 2 Third Avenue SE, Minneapolis, MN 55414, USA. (efi@umn.edu)

D. J. Jerolmack, Department of Earth and Environmental Science, University of Pennsylvania, Hayden Hall, 240 S. 33rd Street, Philadelphia, PA 19104, USA.